Geophysical Journal International

Geophys. J. Int. (2010) **181,** 1077–1092 doi: 10.1111/j.1365-246X.2010.04558.x

Multipathing, reciprocal traveltime fields and raylets

N. Rawlinson, M. Sambridge and J. Hauser

Research School of Earth Sciences, Australian National University, Canberra ACT 0200, *Australia. E-mail: nicholas.rawlinson@anu.edu.au*

Accepted 2010 February 9. Received 2010 February 8; in original form 2009 November 16

SUMMARY

A new theory for the calculation of later seismic arrivals in heterogeneous media is presented. We introduce the concept of a 'raylet', which is a segment of a later arriving ray path between source and receiver defined by joint properties of forward and reciprocal traveltime fields. We show that all rays between a single source and receiver in arbitrary heterogeneous media can be divided into a unique set of raylets, any one of which can be used to construct the complete two-point path. A particularly useful property of raylets is that they correspond to stationary curves in the summed (forward and reciprocal) traveltime fields, i.e. adding the first (or second, or even later) arriving traveltime field from some point A to the first (or second, or even later) arriving traveltime field from some point B. We show that many raylets, each corresponding to a later arriving phase, require only earlier arrival traveltime fields for their construction. The theory describing the properties of raylets is the primary result of the paper. One practical consequence is that many later arrivals between source and receiver in heterogeneous media can be found from just two first-arrival traveltime fields, one from the source and the other (the reciprocal field) from the receiver.

The theory and a method for constructing later arrivals is demonstrated though numerical experiments in 2-D but holds without change in 3-D. We use a simple grid-based eikonal solver to compute forward and reciprocal first-arrival traveltime fields, and validate our results with a ray-based wave front construction (WFC) technique. In one test involving a simple wave front triplication (or swallowtail), all three arrivals are retrieved. In another example featuring severe velocity heterogeneities, 16 out of a total of 37 arrivals are found. The theory shows that combining second and higher order traveltime fields from source and receiver yields all raylets and hence all later arrivals. In practice only first-arrival traveltime fields are usually available and for this case we describe a simple procedure to find any remaining arrivals using intermediate artificial sources together with their first-arrival traveltime fields. The properties of raylets and their manifestation in the joint traveltime field appears to be a previously unrecognized feature and provides a novel new approach to the calculation of later arrivals.

Key words: Numerical solutions; Computational seismology; Theoretical seismology; Wave propagation.

1 INTRODUCTION

In geometric ray theory, multipathing can be simply defined as the existence of more than one ray path connecting two points in a medium. The term is usually applied when smooth velocity variations cause propagating wave fronts to focus and eventually self-intersect (or triplicate), thus producing later arriving rays. This phenomenon is distinct from the production of multiple phases by reflection and transmission at velocity discontinuities, although undulations in interface topography can also cause wave front focusing, and hence multipathing. In seismology, the effects of multipathing can be observed in seismograms (e.g. Capon 1971): wavetrains tend to become longer and more convoluted, but it is difficult to discriminate between different arrivals, and separate geometric spreading effects from finite frequency effects like scattering. Partly for these reason, many applications that use geometric ray theory for data prediction, such as seismic tomography, reflection migration, and earthquake location, do not exploit later arriving information. An added complication is that the computation of multiple two-point paths is a nontrivial problem that is much more difficult to solve than the problem of simply locating first-arrivals.

Due to the important role played by geometric ray theory in modern seismology, a wide variety of techniques and algorithms have been proposed to solve the two point problem of finding a path and associated traveltime between a source and a receiver in heterogeneous media. These can generally be classified as either ray

based or grid-based (see Červený 2001; Rawlinson *et al.* 2007, for comprehensive descriptions and reviews). The ray based approaches can be split into those that solve an initial value problem and those that solve a boundary value problem. The former include shooting methods (e.g. Julian & Gubbins 1977; Farra & Madariaga 1988; Sambridge 1990; Velis & Ulrych 1996; Rawlinson *et al.* 2001), in which the trajectory of some initial path is iteratively adjusted until it hits the receiver, and the latter include bending methods (e.g. Julian & Gubbins 1977; Pereyra *et al.* 1980; Um & Thurber 1987; Zhao *et al.* 1992; Koketsu & Sekine 1998), in which the geometry of an arbitrary curve connecting source and receiver is iteratively adjusted until it satisfies Fermat's principle of stationary time. Both classes of technique are widely used, and can in theory locate more than one arrival in continuous media. However, the severe nonlinearity of the two-point problem in the presence of structure that gives rise to multipathing means that ray shooting and bending methods are not practical for tracking later arrivals.

An alternative approach to ray tracing is to compute traveltimes to a grid of points that span the medium. Implicitly, the complete traveltime field contains the wave front geometry as a function of time, and all possible ray trajectories. Two common grid-based schemes include finite difference solution of the eikonal equation and shortest path ray tracing (SPR). Eikonal solvers use finite difference stencils and causality to propagate a computational front outward from the source, either as an expanding square (Vidale 1988, 1990; Hole & Zelt 1995; Afnimar & Koketsu 2000) or in the shape of the first-arriving wave front (Qin *et al.* 1992; Cao & Greenhalgh 1994; Sethian & Popovici 1999; Rawlinson & Sambridge 2004b). Instead of solving a differential equation, SPR uses a network or graph formed by connecting neighbouring nodes with traveltime path segments. The traveltime field is computed by tracking first-arrival ray paths outward from the source using Djikstra-like algorithms (Nakanishi & Yamaguchi 1986; Moser 1991; Fischer & Lees 1993; Cheng & House 1996; Zhao *et al.* 2004). Eikonal solvers and SPR can be very robust and efficient in the presence of significant heterogeneity, but cannot track later arrivals in continuous media.

The first successful schemes capable of computing all arrivals were published nearly two decades ago (Sun 1992; Vinje *et al.* 1993), and involve the progressive advance of a wave front, described by a set of points, though smoothly varying 2-D media. Initial value ray tracing is used to update the points by a given time step, and new points are introduced where necessary using interpolation to avoid under-sampling of the evolving wave front. This basic idea, often called wavefront construction or WFC, has been extended and applied to 3-D continuous models (Vinje *et al.* 1996; Lucio *et al.* 1996; Chambers & Kendall 2008) and more complex models that include interfaces (Vinje *et al.* 1999). The introduction of a phase-space criterion for interpolating new points (Lambaré *et al.* 1996; Hauser *et al.* 2008) greatly improves the robustness of the scheme. To date, WFC has proven to be the most practical scheme developed so far for tracking multi-arrivals. It is commonly used in the exploration industry, including for migration of reflection data (Ettrich & Gajewski 1996; Xu & Lambaré 2004; Xu *et al.* 2004), and has been used as the forward solver in multi-arrival traveltime tomography (Hauser *et al.* 2008).

In the last decade or so, the development of grid-based multi-arrival schemes has rapidly expanded, due largely to the efforts of the computational mathematics community. One approach is to partition the multivalued traveltime field into a series of single valued domains, in which fast and efficient first-arrival solvers can be applied (Benamou 1996; Bevc 1997; Benamou 1999; Symes & Qian 2003). The main difficulty is to identify a robust splitting strategy for isolating single-valued domains, because there is no prior knowledge of the structure of the multivalued field. Level set methods (Osher & Sethian 1988), commonly used in fluid dynamics (Mulder *et al.* 1992; Chang *et al.* 1996), can also be applied to track multi-arrivals (Osher *et al.* 2002; Leung *et al.* 2004; Cockburn *et al.* 2005), although the wave front needs to be represented by the projection of the intersection between two zero level set surfaces in 3-D reduced phase space, which is potentially time consuming (and this is only for 2-D problems). Despite this, recent work by Cheng (2007) indicates that it is on the verge of being computationally feasible in seismic tomography.

Other grid-based multi-arrival techniques include the 'fast-phase space' method of Fomel & Sethian (2002) who solve a system of time independent partial differential equations derived from the Liouville formulation of the kinematic ray tracing equations; the 'segment projection' method of Engquist *et al.* (2002) which explicitly tracks a wave front described by a contiguous set of line segments in reduced phase space; and dynamic surface extension (DSE) (Steinhoff *et al.* 2000), which implicitly tracks wave front evolution on a grid of points, each of which carry the coordinate of the closest point on the wave front. Other methods also exist (see Benamou 2003; Engquist & Runborg 2003, for comprehensive reviews), but so far, none have proven to be as robust and efficient as WFC.

The focus of this paper is not on computational techniques for later arrivals *per se*, but rather on how information on later arrivals is contained in the combination of forward and reciprocal traveltime fields. In particular, we show how every path connecting a source and receiver in smoothly varying media can be broken down into a unique set of segments, that we call 'raylets'. Each raylet is a consequence of the overlap of two traveltime fields, one emanating from the source and another from the receiver. First, second or later arriving traveltime fields may be combined with each other to form raylets. The key point is that each raylet corresponds to a short valley or ridge along which the summed forward and reciprocal travel field is stationary with respect to position. These stationary raylets can be identified from the corresponding traveltime fields and as a result the entire ray path constructed. As will be shown, a convenient property is that all arrivals between a fixed source and receiver are built from raylets that require only 'lower' order (or earlier arrival) traveltime fields. We show 2-D examples where the combination of two first-arrival traveltime fields, obtained with a standard eikonal solver, may be used to generate multiple arrivals—in one case with a complex medium, up to 16 are obtained. A WFC technique is used to validate our results. To our knowledge the properties of raylets have not been previously recognized, but allow a novel approach to the calculation of multiple arrivals. Although presented in a seismic context, this theory will be equally applicable to other fields that use geometric ray theory, for example ocean acoustics, infrasound and helioseismology.

2 RECIPROCAL TRAVELTIME FIELDS AND RAYLETS

A wave front that emanates from a source point will initially describe a single-valued traveltime field, but as it evolves and interacts with velocity heterogeneity, it may begin to self-intersect, hence producing multipathing. Thus every ray path, regardless of how many other rays might arrive before it at some given receiver, begins as a first-arrival. This is demonstrated in Fig. 1, which shows three

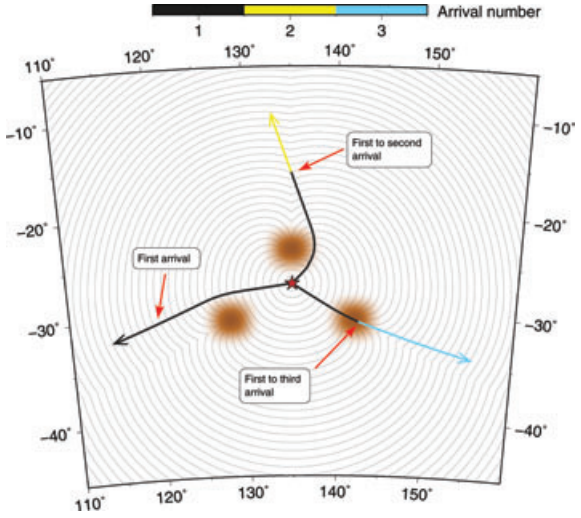

Figure 1. The anatomy of multipathing rays in the presence of velocity heterogeneity. First-arrival wave fronts, contoured at 20 s intervals, are also shown for reference. The first-arrival ray is everywhere perpendicular to the wave front. Later arriving rays begin as first-arrivals, but are eventually overtaken by another portion of the wave front. This can be observed for both the second and third-arrivals—the ray is initially perpendicular to the first-arrival wave front, but then switches to an acute angle when it begins to arrive later.

ray paths emanating from a source point and separately interacting with three low velocity anomalies. One path is clearly a first-arrival along its complete trajectory, as it is everywhere perpendicular to the first-arrival wave front that is also included in the figure as a series of snapshots in time. The two remaining rays begin as first-arrivals, but eventually become later arrivals as other paths begin to arrive along its trajectory at earlier times. This occurs due to the wave front triplicating and forming a swallowtail. The first-arrival wave front shown in Fig. 1 discards all later arrivals, and instead exhibits sharp discontinuities in place of the growing triplication. The ray that becomes a second-arrival clearly passes across one of these discontinuities, at which point it ceases to be perpendicular to the first-arrival wave front. The ray that appears to jump directly from a first to a third-arrival passes though a caustic, which represents a point in space where a triplication initiates (i.e. a focal point). The main concept illustrated in Fig. 1 is that all later arriving rays begin as first-arrivals, and progressively become later as the wave front evolves.

The logical extension of what we observe in Fig. 1 is that an Nth-arrival [where $N > 1$] at some receiver will have begun as a first-arrival, before gradually becoming later and later. In fact, at any point along the two point path, the ray will be an Mth-arrival, where $M = 1, 2, \ldots, N$. Of course, as shown in Fig. 1, it is possible for a ray to jump from an Mth-arrival to an $M + 2$th-arrival, with no intermediate $M + 1$ stage, but this only occurs in the special case of a ray passing through a caustic. Now consider the simple situation illustrated in Fig. 2 (top), which schematically shows a ray path emanating from point A and propagating until it reaches point B. It begins as a first-arrival (A1), eventually switches to a second arrival (A2), before switching to a third-arrival (A3), which is what is detected at point B. The two 'switch' points occur when another part of the wave front starts to arrive earlier than the wave front segment associated with the ray (these are denoted by vertical green bars along the ray). If we now apply the *principle of reciprocity*—that the path traced out by a ray travelling from a

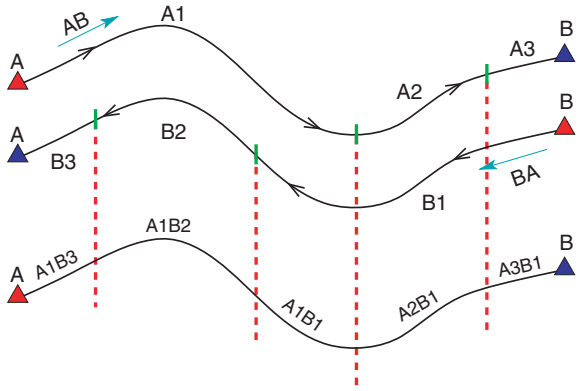

Figure 2. Schematic diagram showing the relationship between reciprocal ray paths (top and middle) propagated between two points A and B. A *raylet* is defined as a segment of the two-point ray path that contains parts of the forward and reciprocal path that do not switch arrival number (bottom). In this case, the complete two-point path comprises raylets A1B3, A1B2, A1B1, A2B1 and A3B1. Vertical green tick marks denote arrival number switch points along forward and reciprocal rays (e.g. when the ray goes from first to second-arrival—see Fig. 1).

source to a receiver is identical to that of a ray travelling from the receiver to the source—it is clear that an Nth-arrival ray traced from A to B will have an identical path to an Nth-arrival ray traced from B to A. This ray will undergo the same evolution in terms of later arrival status (i.e. first-arrival, second-arrival, . . . , Nth-arrival), but obviously, these stages will occur at different places along the path compared to the ray traced from A to B [*cf.* Fig. 2 (middle)]. This is because the (green) change-over points are only a function of the source position at A, and not the receiver position at B.

We introduce the term 'raylet' to facilitate description of the joint properties of spatially identical forward and reciprocal ray paths between a source and a receiver. We define a raylet as a curve in space along which both the forward and reciprocal ray paths do not switch from an earlier to a later arrival type. Raylets are shown schematically in Fig. 2 (bottom), where the path from A to B contains raylets A1B3, A1B2, A1B1, A2B1, A3B1. A raylet, therefore, contains information about the evolution of the forward and reciprocal wave front (or traveltime fields), of which a ray path describes only the trajectory of a single point. It will be convenient to label raylets according to the latest arrival of the contributing segments from the forward and reciprocal rays; thus, A1B1 is a first-order raylet, A1B2 is a second-order raylet and A1B3 is a third-order raylet. In general, an Nth-arrival path is composed of up to $2N - 1$ raylets, since a change from one raylet type to another occurs at every switch point of the forward and reciprocal ray.

3 RAYLET EXTRACTION AND MULTIPATHING

A simple test is performed to show that first-order raylets can be readily extracted from first-arrival traveltime fields which in this case are computed using an eikonal solver known as the fast marching method or FMM (see Sethian 1996; Sethian & Popovici 1999; Popovici & Sethian 2002; Rawlinson & Sambridge 2004b; de Kool *et al.* 2006, for more details). Here FMM is implemented in 2-D spherical shell coordinates (where velocity is a function of latitude and longitude), with radius fixed at 6371 km. Smooth variations in velocity are defined by a mosaic of cubic B-spline velocity patches, the values of which are controlled by a regular grid of velocity

vertices. Although implementation in 3-D would be straightforward, it is much easier to visualize the results in 2-D, and hence clearly demonstrate the principles involved. Furthermore, comparison with other techniques is much simpler to facilitate in 2-D.

Figs 3(a) and (b) shows the first-arrival traveltime field generated from both a source and a receiver in a medium defined by a solitary low velocity anomaly superimposed on a constant background velocity of 4.0 km s^{-1}. In both cases, evidence of a triplication can been seen by the formation of a wave front discontinuity in the neighbourhood of the anomaly, thus indicating the presence of a swallowtail. If we now take the sum of the forward and reciprocal fields (Fig. 3c), a remarkable phenomenon is observed: the joint traveltime surface contains three stationary segments (Fig. 3d), which correspond to three separate first-order raylets. Each first-order raylet is associated with one of three different paths between source and receiver (Fig. 4). Although it is well known that the first arrival will correspond to a minimum curve in the joint traveltime field, to our knowledge, the appearance of other stationary segments has not been previously recognized in the literature. Raylets generally span only a short segment of a ray path, but it is a simple matter to reconstruct the entire path by beginning at any point on the raylet and following the traveltime gradient back to the source and receiver using the forward and reciprocal time fields, respectively. Rawlinson & Sambridge (2004a) describe how this can be done to obtain a source-receiver ray for a single time field; the procedure used here is exactly the same except that it now starts from a point along the raylet and is applied twice. Fig. 4 shows the result of this process, which produces three separate paths, all of which are continuous in gradient at their join points. We refer to this simple scheme for producing later arrivals as the first-order raylet method (FORM).

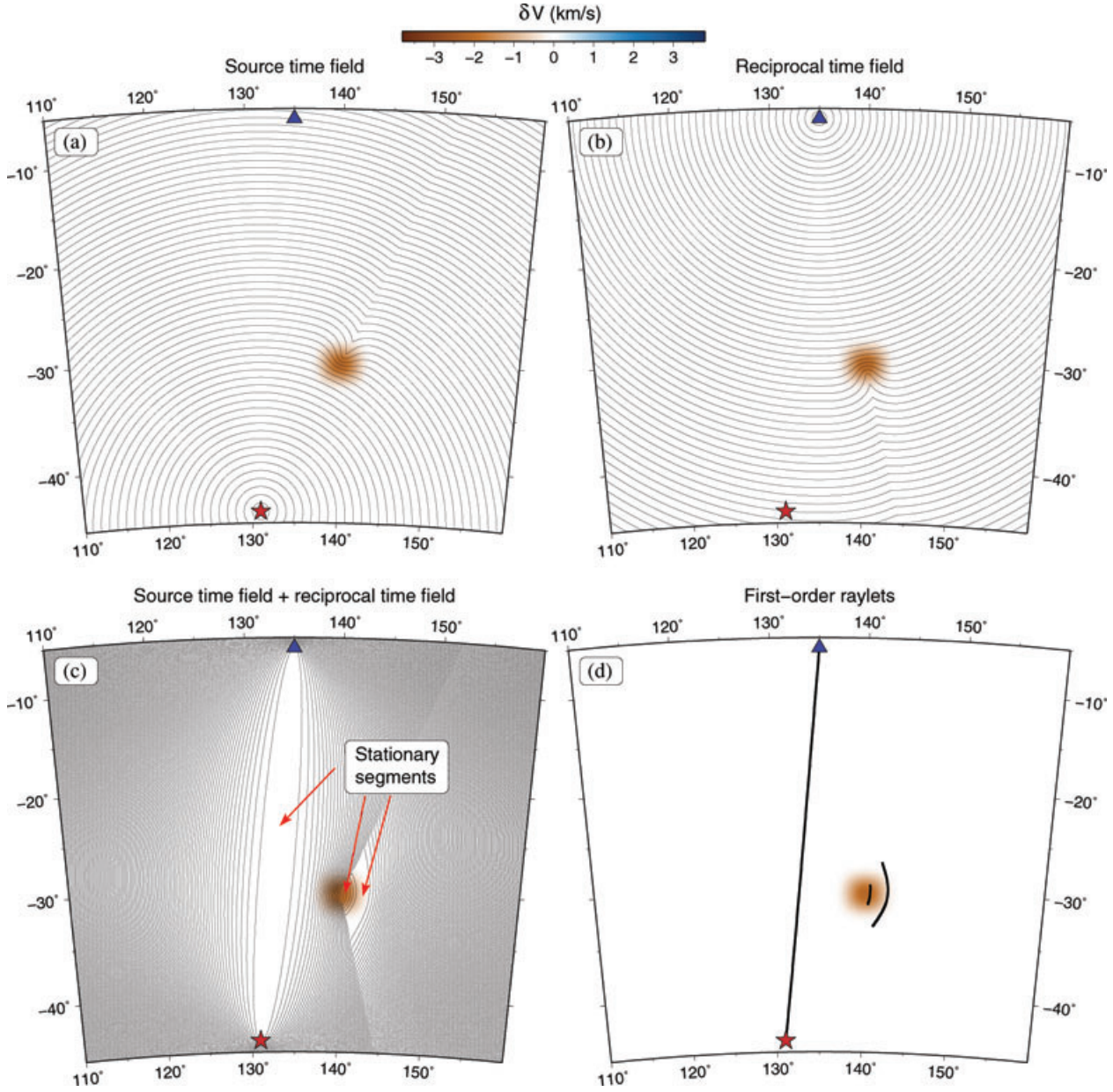

Figure 3. Application of FORM in the presence of a single low velocity anomaly. (a) Source time field; (b) reciprocal time field generated from the receiver point; (c) sum of the source and reciprocal time fields; (d) first-order raylets. The source is denoted by a red star and the receiver by a blue triangle. Wave fronts in (a) and (b) are contoured at 20 s intervals and the sum of the two traveltime fields shown in (c) is contoured at 5 s intervals.

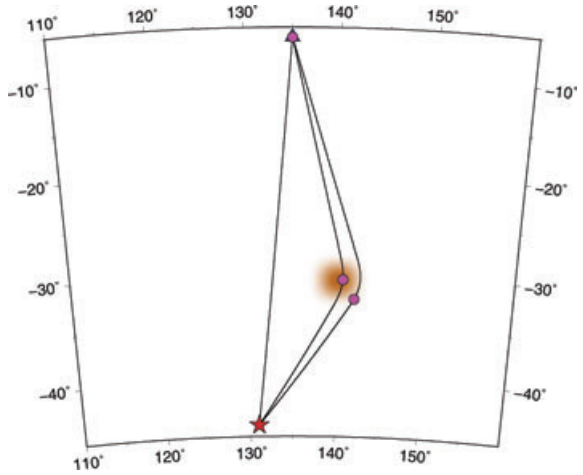

Figure 4. Complete two-point paths obtained by picking a point (magenta dots) along each of the first-order raylets and following the traveltime gradient back to the source and receiver through the forward and reciprocal traveltime fields, respectively.

The intriguing results contained in Figs 3 and 4 are verified using the WFC method of Hauser *et al.* (2008), which is based on local ray tracing and interpolation in phase space. WFC is robust and computationally efficient in 2-D media, and is capable of predicting all arrivals. Fig. 5a shows the complete triplicating wave front generated by the low velocity anomaly, as calculated by WFC. As expected, the wave front passes through the receiver three times, and the ray paths correspond exactly to what is predicted by using raylets (Fig. 5b). WFC is also used to track the evolution of rays from the source to the receiver (Fig. 5c) and the receiver to the source (Fig. 5d) in terms of their arrival status in the source and reciprocal traveltime field, respectively (*cf.* Fig. 2). The superposition of these two sets of rays (Figs 5e and f) clearly reveals the presence of three first-order raylets, all of which correspond exactly to those in Fig. 3(d).

3.1 The stationarity of raylets

The aforementioned example demonstrates that first-order raylets can be found with just two first-arrival traveltime fields. This can be generalized by considering the following situation. Let A and B be two separate points in a smooth velocity medium of arbitrary complexity. Now consider two rays, one emanating from A and the other emanating from B, and let C be their point of intersection (see Fig. 6a). The two path segments AC and CB are true ray paths in the sense that they satisfy Fermat's principle of stationary time and may be first or later arrivals. However, the complete path ACB will not automatically be a ray path because stationarity is not guaranteed for point C. If T_{AC} and T_{BC} are the traveltimes along segments AC and CB, respectively, then the total traveltime is simply given by

$$T_{AB} = T_{AC} + T_{CB}. \tag{1}$$

According to Fermat's principle, the path ACB will be stationary provided:

$$\frac{\partial T_{AB}}{\partial \mathbf{x}_C} = \nabla_{\mathbf{x}_C} T_{AB} = \nabla_{\mathbf{x}_C} [T_{AC} + T_{CB}] = 0, \tag{2}$$

where $\mathbf{x}_C$ is the position of C. If we have traveltimes computed from A and B to all points in the medium, then any point C that satisfies Equation 2 must correspond to extrema of the summed fields $T_{AC} + T_{CB}$. Since this argument does not specify which traveltime field from A is summed with that from B, any pair of fields may be used, for example first-arrival field from A may be summed with the second-arrival field from B and so on. In each case, all stationary points must lie on rays between A and B, and it turns out that they delineate segments corresponding to where $\nabla T_{AC} = -\nabla T_{CB}$, that is where the forward and reciprocal paths overlap. Hence we arrive at the main conclusion which is that each raylet corresponds to a stationary segment of the summed traveltime field.

In the simple triplication example shown in Fig. 3, all the stationary points C trace out three first-order raylets. As the argument above implies, two first-arrival traveltime fields can only yield first-order raylets (but all associated later arrivals), because they exist only when the first-arrival wave fronts of the forward (Fig. 3a) and reciprocal (Fig. 3b) fields are parallel (Fig. 3d). The first-order raylet for the first-arrival path is a global minimum curve which connects the source and receiver for the simple reason that the corresponding forward and reciprocal rays never become later arrivals. For the second and third arrivals, this is not the case, which is why their first-order raylets are much shorter.

4 TOWARDS THE LOCATION OF ALL ARRIVALS

Using two first-arrival traveltime fields, we have shown that it is possible to extract all first-order raylets and their associated later arrival paths. However, in media of arbitrary complexity, it is not clear how many later arrivals might contain first-order raylets. To gain insight into this problem, we repeat the numerical experiments carried out earlier (Figs 3–5) using a model containing two low velocity anomalies instead of one (see Fig. 7). The position of these anomalies relative to the source and receiver result in two traveltime field discontinuities forming for both the forward and reciprocal traveltime fields (Figs 7a and b). The summed time fields (Fig. 7c) reveals the location of six stationary segments which correspond to the presence of six first-order raylets (Fig. 7d). The associated ray paths are shown in Fig. 8. Using WFC, the complex nature of the evolving wave front (Fig. 9a) can be explained by the fact that each branch of the initial triplication, formed as a result of interaction with the anomaly closest to the source, is then triplicated again to produce a total of nine arrivals (Fig. 9b). Since only six of the nine paths correspond to stationary segments in the summed first-arrival field, this implies that three of the arrivals do not contain first-order raylets.

Figs 10 and 11 show the arrival evolution of all nine forward and reciprocal rays using WFC. Fig. 10 clearly reveals the presence of first-order raylets in the first six arrivals (*cf.* Fig. 7d), and Fig. 11 shows the absence of first-order raylets for the last three arrivals. In the case of arrivals seven and eight, the lowest-order raylets are second-order (A1B2 and A2B1, respectively), and hence to find these arrivals a first-arrival traveltime field from A must be added to a second-arrival traveltime field from B or vice versa. The ninth-arrival requires calculation of a third-arrival traveltime field from either A or B in addition to a reciprocal first-arrival traveltime field, since the lowest order raylets are third-order (A3B1 and A1B3).

In the absence of a practical grid-based approach for generating later-arriving traveltime fields (and hence readily computing higher-order raylets) the question arises as to whether it is possible to locate all arrivals using only first-arrival traveltime fields. If we return to the idea, encapsulated in Equation 2, of forming a composite ray from two separate rays by applying Fermat's principle of stationary time, then it is quite straightforward to see that this can be applied

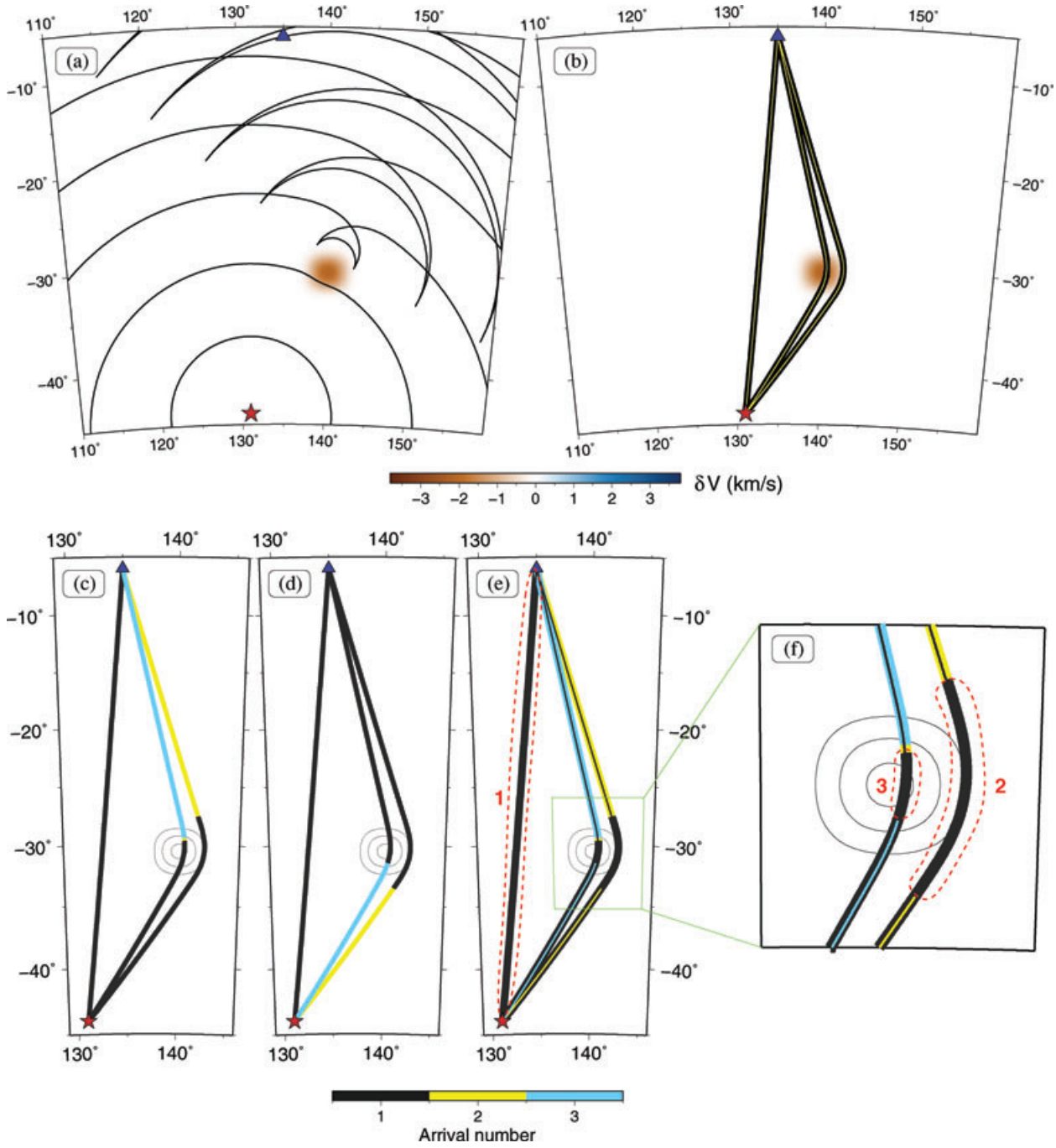

Figure 5. Application of WFC in the presence of a single low velocity anomaly. (a) Snapshots of the complete multi-valued wave front (at 200 s intervals); (b) FORM ray paths (yellow) from Fig. 4 superimposed on WFC ray paths (black); (c) rays propagated from the source; (d) rays propagated from the receiver; (e) reciprocal rays superimposed on the source rays; (f) magnified region of (e) showing the presence of first-order raylets in the second and third-arrival paths. The source is denoted by a red star and the receiver by a blue triangle.

to any number of ray segments. For instance, if we insert a point Q between A and C and a point P between C and B (see Fig. 6b), then the path AQCPB would be a valid ray path provided:

$$\nabla_{\mathbf{x}_Q}[T_{AQ} + T_{QC}] = \nabla_{\mathbf{x}_P}[T_{CP} + T_{PB}] = \nabla_{\mathbf{x}_C}[T_{QC} + T_{CP}] = 0. \tag{3}$$

This extension to the theory could be used to address a situation like that schematically illustrated in Fig. 12(a). which shows a path between A and B with no first-order raylet. If a point C along the ray path can be found (Fig. 12b), then computing forward and reciprocal traveltime fields between A and C and C and B may yield raylets A1C1 and C1B1. The 'trick', of course, is to find the point C. A simple but rather time consuming way of doing this is to compute traveltime fields from sources placed at every point in the grid. By doing so, forward and reciprocal fields will exist between A, B and all candidate points C. For a particular point on the grid, a valid traveltime to both A and B could be obtained by summing the traveltime field generated from that point with the A field and B field, respectively, and searching for stationary curves. If these two traveltimes were then summed and gridded throughout the medium,

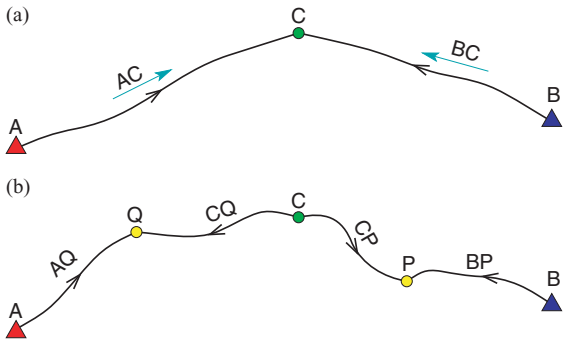

Figure 6. Schematic illustration of how independently computed ray segments can be stitched together by applying Fermat's principle of stationary time to their intersection points. (a) The path ACB is a valid ray path provided $T_{AC} + T_{BC}$ is stationary for some point C; (b) the path AQCPB is a valid ray path provided $T_{AQ} + T_{QC}$, $T_{CP} + T_{PB}$ and $T_{QC} + T_{CP}$ are all stationary.

then stationary curves of the new field would correspond to valid C points. Thus, whereas no A1B1 raylet may exist, the two-point path could be reconstructed from raylets A1C1 and C1B1. If the addition of a single point between A and B is not sufficient to detect all arrivals, then extra points could be inserted between A and C and C and B, and the same procedure followed. Ultimately, any number of points could be inserted in this fashion. In principle, this recursive approach must eventually detect all two point arrivals between A and B, because any ray path can be divided up into a series of first-arrival paths.

Fig. 13 demonstrates how the ninth-arrival from the double triplication example (Figs 7–11) can be constructed in this manner. The central point C can be found using a simple grid search, which must assess all combinations of traveltime fields between A and C and B and C (nine in the case of Fig. 13) to find a stationary point. This is equivalent to matching the gradients of each path in Fig. 13 (left) with each path in Fig. 13 (right) at the join point C. The complete two-point path between source and receiver is composed of four

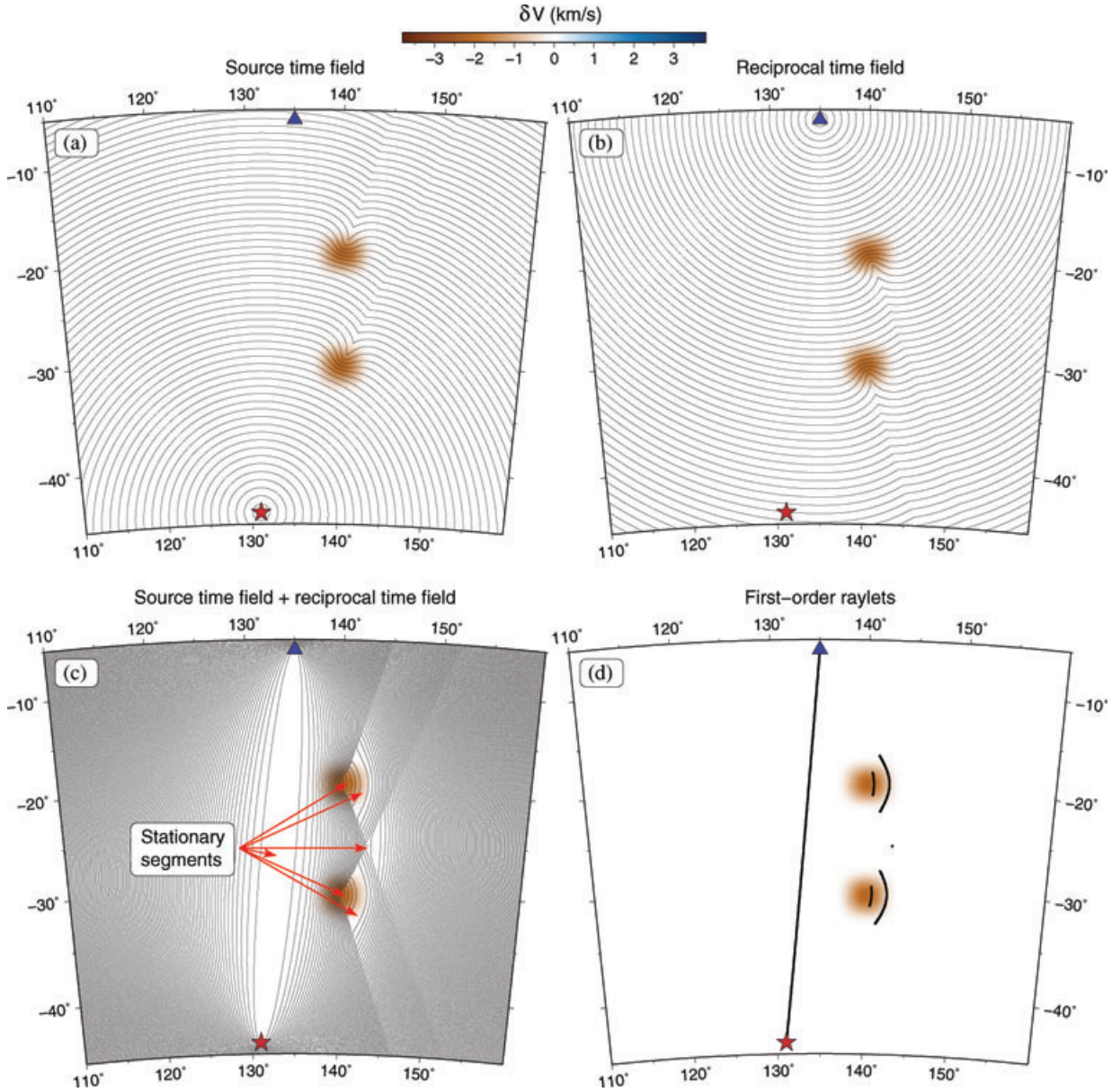

Figure 7. Application of FORM in the presence of two low-velocity anomalies. Refer to the Fig. 3 caption for a description of each plot.

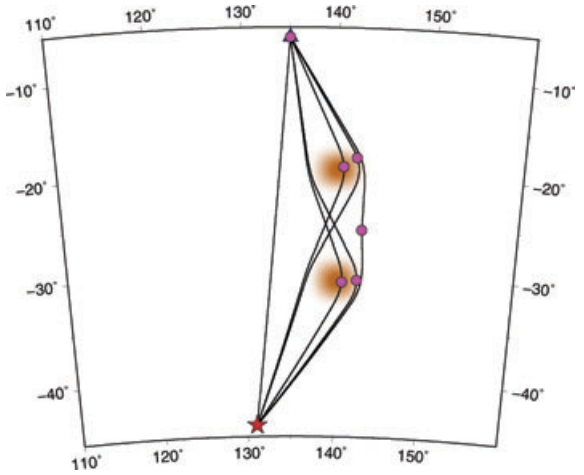

Figure 8. Complete two-point paths obtained from the reciprocal traveltime fields (see Fig. 4 caption for more details).

first-arrival segments. The development of a more efficient scheme for locating multiple stationary points is beyond the scope of this paper, although the matter will be considered further in Section 7.

5 APPLICATION OF THE FORM TO A STRONGLY HETEROGENEOUS MODEL

The preceding examples have shown how first-order raylets can be used to find later arrivals in relatively simple velocity media. We now apply FORM to a strongly heterogeneous model to see what proportion of arrivals are found. The model setup is similar to the previous examples, except that now the background model has a value of 5.0 km s^{-1}, and random perturbations of up to ± 2 km s^{-1} (or ± 40 per cent) are used to generate a large number of multiple arrivals between a single source and receiver. The source (Fig. 14a) and reciprocal (Fig. 14b) traveltime fields both exhibit numerous wave front discontinuities which imply the presence of multiple triplications. Summing together the two fields (Fig. 14c) reveals a complex pattern of first-order raylets (Fig. 14d). By locating points along each of these raylets and tracking back through the time fields as in the previous examples, we recover a total of 16 two-point ray paths (Fig. 15). These span a time range of 56.3 s, from 958.5 s to 1014.8 s.

The complexity of the complete wave front propagated from the source using WFC is shown in Fig. 16a; multiple swallowtails are clearly evident, and the intense folding of the wave front in the neighbourhood of the receiver explains the large number of arrivals. In this case, 37 two-point paths are located (Fig. 16b), 21 of which must contain only higher order raylets. A comparison of the ray paths (Fig. 16d) indicates that the two methods closely agree when equivalent arrivals are considered. The range of all 37 arrivals is 60.9 s, from 958.5 s to 1019.4 s. In general, the arrivals appear to cluster in time (usually in threes) separated by very small traveltimes (less than 0.5 s), which probably correspond to the arrival of triplications formed near the receiver or triplications created by fine-scale anomalies. As such, FORM tends to identify the first branch but not the others, as they correspond to triplicated triplications. One could therefore argue from a finite frequency point of view that the subsequent branches of the triplication could not be detected on realistic seismograms. Of course, whereas this appears to apply quite well to this example, it may not apply generally.

In this example, first-order raylets are used to locate 43 per cent of the arrivals found by WFC, which is designed to find all arrivals. However, as Fig. 16d shows, there is one arrival found by FORM that appears to have eluded WFC. Examination of where this ray lies with respect to the propagating wave front reveals that it is at the very edge of a triplication (i.e. where the second and third-arrival branches intersect). Significantly increasing the number of initial points used by WFC to define the wave front leads to the recovery of this path, but at significant extra computational cost.

6 ACCURACY AND COMPUTE TIME

A simple comparison is made between WFC and FORM (as implemented in the aforementioned examples) in terms of accuracy and

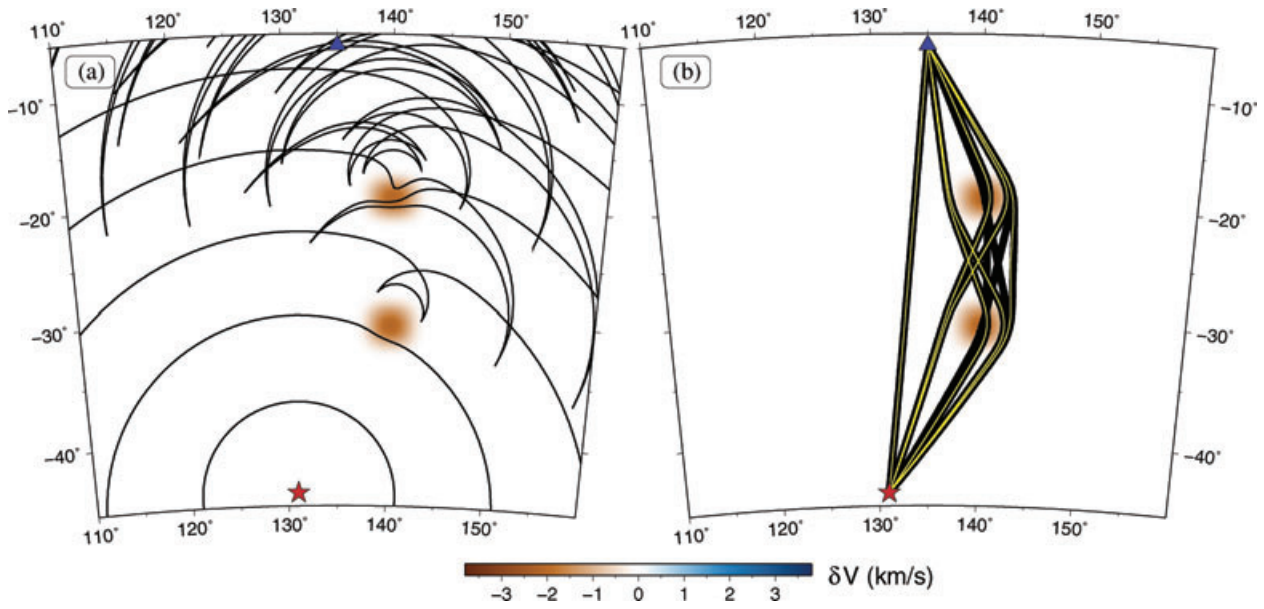

Figure 9. Application of WFC in the presence of two low-velocity anomalies. (a) Snapshots of the complete multi-valued wave front (at 200 s intervals); (b) FORM ray paths (yellow) from Fig. 8 superimposed on WFC ray paths (black).

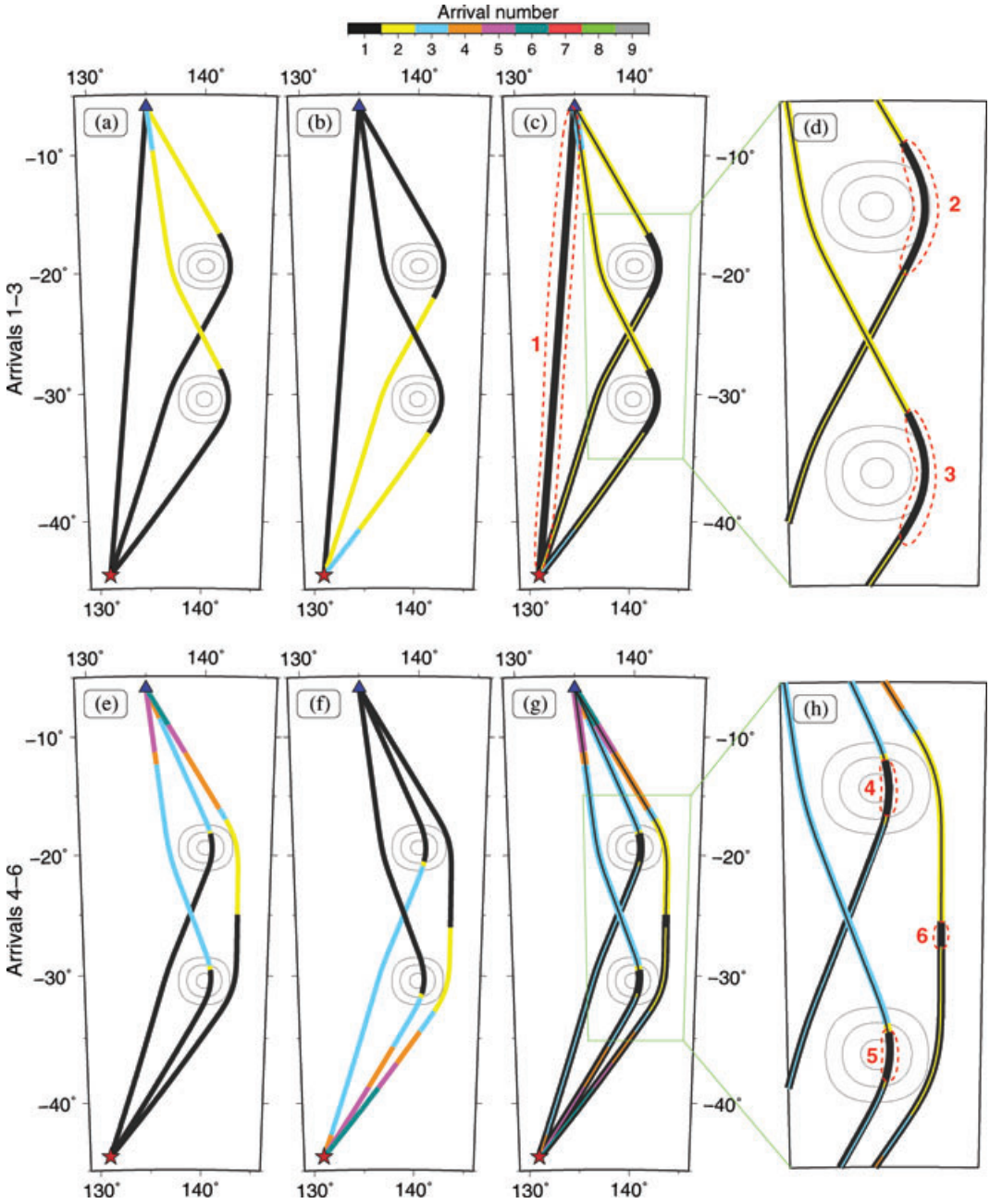

Figure 10. Raylet structure of arrivals 1–3 (top) and 4–6 (bottom) corresponding to the twin low velocity anomalies. The magnified plots (d and h) highlight the presence of first-order raylets contained in arrivals 1–6 (*cf.* Fig. 7d).

compute time. We emphasize that the aim of the paper is to explain the properties of raylets and show that they can be extracted from reciprocal traveltime fields; a raylet-based multi-arrival method is merely a by-product of this goal. Therefore, the purpose of this section is to demonstrate that FORM is a potentially useful way of exploiting raylets, rather than to make a comprehensive comparison with a particular wave front tracking scheme such as WFC. In any case, a fair comparison is difficult because the strengths of the two approaches lie in different areas. WFC can find all arrivals, and only requires one wave front to be propagated to cover a medium with a grid of multivalued traveltimes. On the other hand, extension to 3-D is nontrivial and the traveltime field is irregularly sampled, making it more difficult to compute arrival times at a receiver and their associated two-point paths. FORM uses a regular grid of traveltimes, is straightforward to implement in 3-D, and ray paths are simple to compute retrospectively; however, in its current implementation, the location of all later arrivals is not guaranteed, and one time field must be computed for each source and receiver.

FORM uses mixed-order finite differences (up to second-order) to compute traveltimes, and grid refinement is implemented to account for strong wave front curvature in the neighbourhood of the source (Rawlinson & Sambridge 2004b). Both accuracy and compute time are a function of the total number of grid points used to define the medium. WFC uses a fourth-order Runge–Kutta scheme to locally trace rays from each wave front surface, and a weighted average scheme to interpolate new points in phase space (Hauser

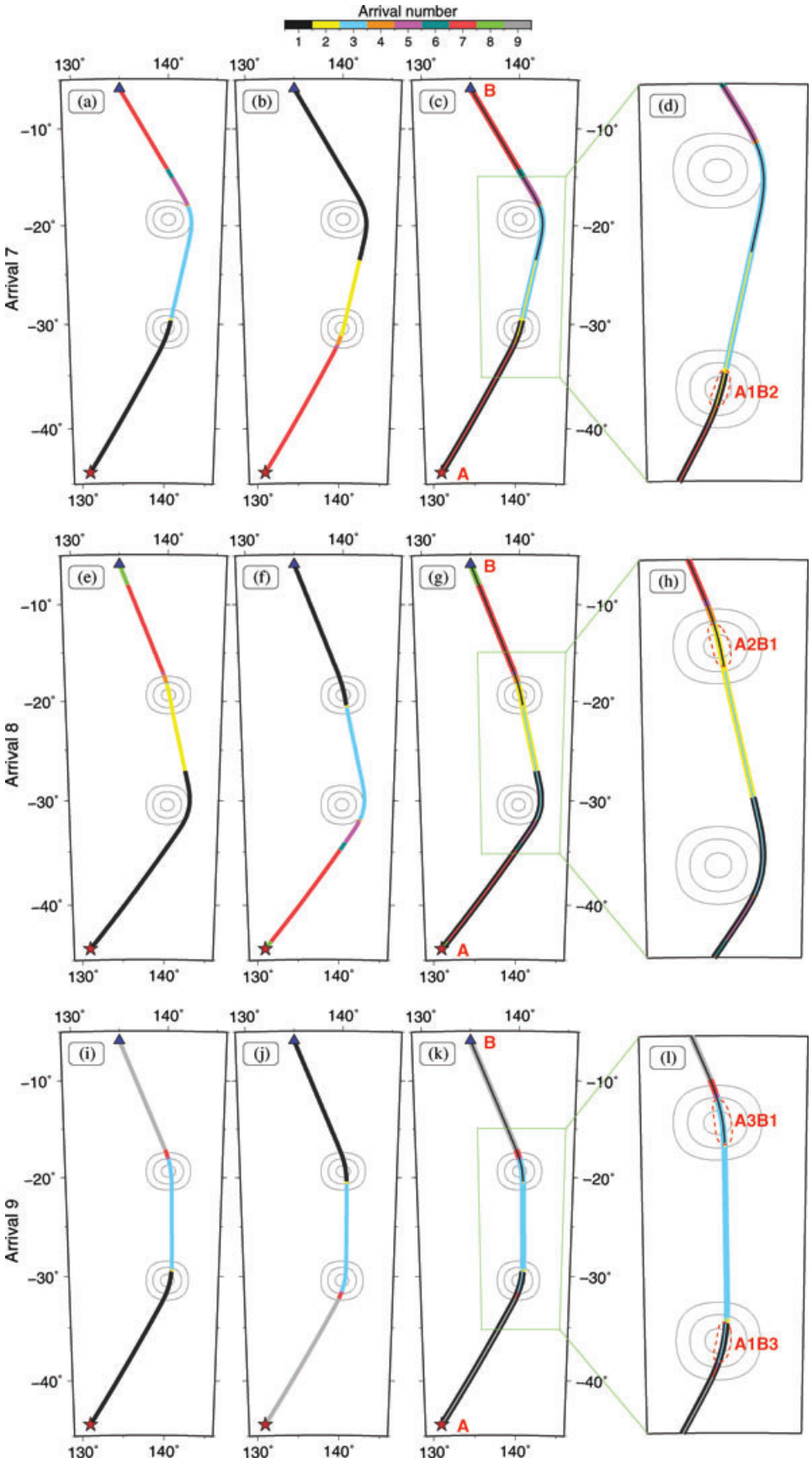

Figure 11. Same as Fig. 10 but now showing arrivals 7–9. The absence of first-order raylets explains why FORM does not recover these rays. The magnified plots (d, h and l) show segments of the ray containing raylets of the lowest arrival number. A and B denote the source and receiver locations, respectively.

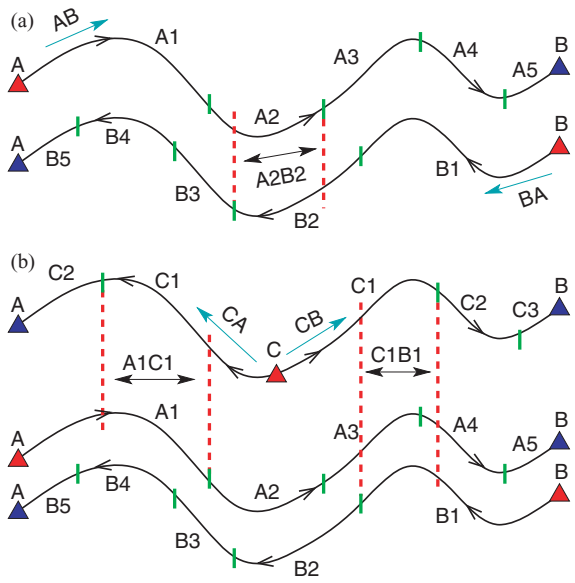

Figure 12. Schematic diagram showing the relationship between reciprocal ray paths propagated between two points A and B (*cf.* Fig. 2). (a) A fifth-arrival that contains no first-order raylet. The earliest arrival raylet is A2B2, which implies that a second-arrival traveltime field is needed to construct a fifth-arrival ray. (b) Computing a new traveltime field from a point C inserted along the ray allows the complete path to be constructed from two first-order raylets (A1C1 and C1B1).

et al. 2008). In this case, accuracy and compute time are largely a function of time step (the time interval between which wave fronts are constructed), and the number of points used to describe the wave front at the source.

We compare the two schemes using the double triplication example shown in Figs 7 to 11. Although nine arrivals are present, only the traveltimes of the first six are used, due to FORM exploiting first-order raylets only. Table 1 shows a comparison between three FORM runs and three WFC runs using different parameter values (see right column of table). In the case of FORM, grid size is progressively halved, which results in CPU time increasing by approximately a factor of four each time. The WFC parameters are chosen to produce approximately equivalent CPU times, which can be achieved by progressively halving the time step and doubling (approximately) the number of points sampling the wave front at the source. All traveltimes are expressed in differential terms using the traveltimes from a WFC run with very small time step and a large number of initial points as a reference (see bottom line of Table 1).

Clearly, FORM1 that uses the coarsest grid, has much smaller traveltime differences than WFC1 (implying much greater accuracy), even though they have similar CPU times. This is also true of FORM2 (compared to WFC2) and to a lesser extent FORM3 (compared to WFC3). The fact that the FORM results do not monotonically converge in all cases can probably be attributed to the fact that the reference times are not an ideal proxy to the exact solutions. The stability of the FORM is a function of the stability of FMM, and previous papers (e.g. Rawlinson & Sambridge 2004a) clearly demonstrate the monotonically convergent behaviour of FMM even in highly heterogeneous media. WFC may not be as stable, and given the small differences between FORM1 and the reference time, it appears that they share a similar level of accuracy. Regardless of the reason for the traveltime behaviour seen in Table 1, it is clear that our simple FORM scheme is capable of producing very accurate results—more accurate in many cases than WFC and with less CPU time.

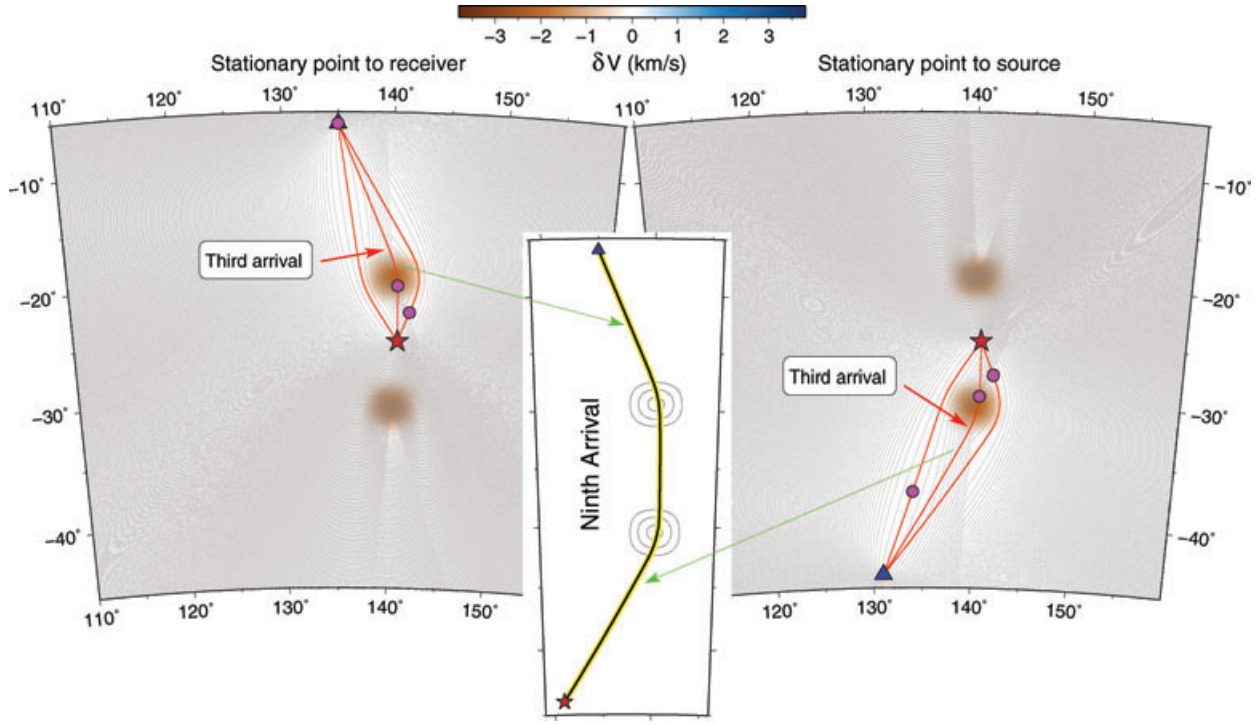

Figure 13. Example showing how additional traveltime fields can be used to obtain more later arrivals. In this case, a traveltime field computed from a point inserted between the source and receiver is summed with traveltime fields computed at the receiver and source. Stationary curves obtained from each of these processes gives rise to three paths. The slowest ray in each case is tangent at the new point (denoted by a red star), thus recovering the ninth-arrival featured in Fig. 11.

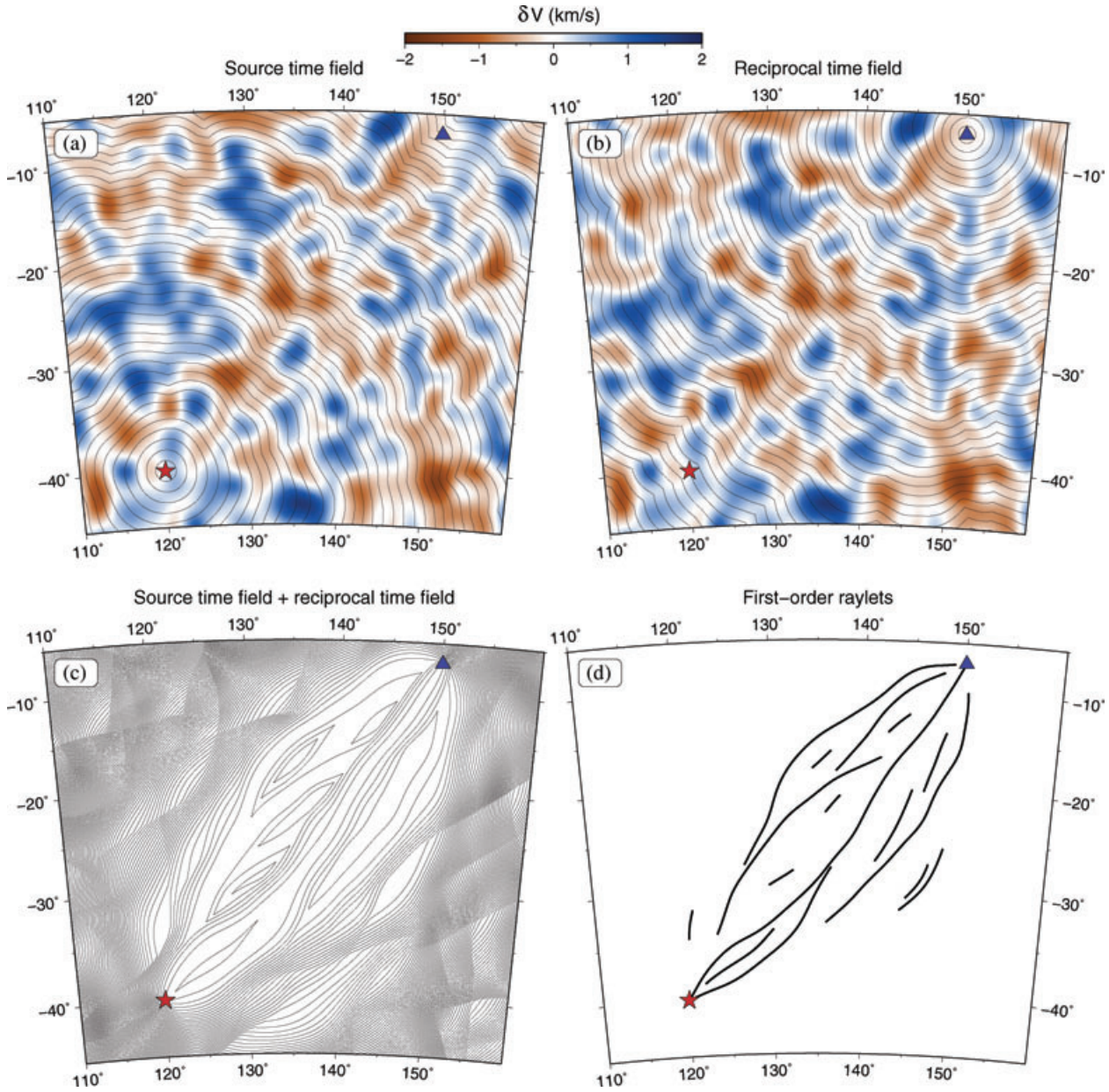

Figure 14. Application of FORM in the presence of a complex velocity model. Refer to the Fig. 3 caption for more details.

7 DISCUSSION AND CONCLUSIONS

The main result of this paper is the concept of a raylet, which is a segment of a two-point path that contains information on the multivalued nature of both the forward and reciprocal traveltime fields, and can be used to locate later-arrivals in heterogeneous media. For an Nth-arrival traveltime, the associated path can be decomposed into as many as $2N - 1$ raylets. Each raylet contains overlapping segments of the forward and reciprocal ray path whose arrival numbers, in the context of the evolving traveltime field, are invariant. In general, an Mth-order raylet [where $M \leq N$] must contain at least one ray segment that is an Mth-arrival, the other being of less or equal arrival number. The significance of raylets is that they provide sufficient information about later arrivals that it is possible to recover them using earlier arrival information from forward and reciprocal traveltime fields. Thus, if a third-arrival path evolves from source A to receiver B as A1, A2, A3, and the reciprocal path as B1, B2, B3 and the first-order raylet A1B1 exists, then the complete ray path from A to B can be computed with only a knowledge of first arrival ray-fields (or traveltime fields) generated at A and B.

Motivated by this phenomenon, we develop a simple raylet-based scheme which uses a first-arrival eikonal solver to compute the forward and reciprocal traveltime fields. Although this automatically limits us to the detection of first-order raylets, it is sufficient to demonstrate the basic principles involved. Using a simple model featuring a solitary low velocity anomaly, we show that the stationary curves present in the summed forward and reciprocal traveltime fields correspond exactly to all first-order raylets (Figs 3–5). Beginning at any point along these raylets, we show that it is possible to obtain the complete ray path by following the traveltime gradient back to the source and receiver through the

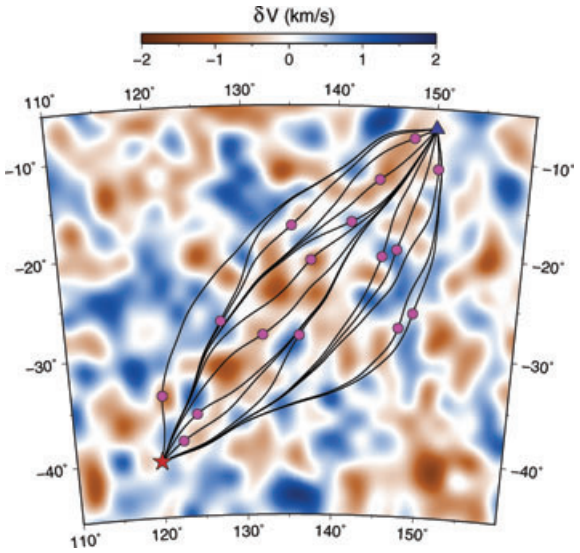

Figure 15. Complete two-point paths obtained from the reciprocal traveltime fields (see Fig. 4 caption for more details).

forward and reciprocal fields, respectively, thus yielding all three arrivals.

In more complex models, not all arrivals can be found in this way for the simple reason that first-order raylets appear not to exist for paths that experience multiple triplications. We demonstrate (Fig. 13) that even in this case, it is possible to recover the complete ray path by using the reciprocity principle with only first-arrival traveltime fields. The basic idea is to introduce new points along the ray path, found using a grid search for example, from which traveltime fields are generated and coupled with those already computed from the source and receiver. This branch decomposition approach allows rays to be pieced together from a series of first-arrival segments. A basic grid-search approach for finding all arrivals with first-order raylets is simple to implement, but has the potential to become computationally prohibitive if many levels of triplication occur. Although the development of more efficient schemes is beyond the scope of this paper, it may be possible to drastically reduce the search area (for example, higher levels of triplications in the source and reciprocal fields are unlikely to occur in the vicinity of the source and receiver, respectively) or use more efficient spatial sampling techniques like the Neighbourhood Algorithm or NA (Sambridge 1999a,b). Even so, we have shown that a simple FMM-based FORM can capture a significant portion of later arrivals with an efficiency and accuracy that in some cases exceeds WFC—currently the state-of-the-art method for computing seismic multipathing.

The idea of using reciprocity to find later arrivals has been considered previously in seismology; for example, it is quite well known in the literature that later arriving reflections can be found by computing traveltimes from the source to the interface and from the receiver to the interface, adding the results, and then locating stationary points (e.g. Williamson 1990; Matsuoka & Ezaka 1992; Riahi & Juhlin 1994). In fact, Matsuoka & Ezaka (1992) also recognize that summing together a source and a reciprocal first-arrival traveltime field in smooth velocity media yields the first-arrival path as a global minimum curve. However, they do not recognize that stationary curve segments, which appear when two-point multipathing is present, can be used to compute later arrivals. In media with discontinuities, a raylet-based method could be readily applied to find multipathing phases which reflect or refract at interfaces. This scenario is similar to that of inserting an additional point in the medium between source and receiver to locate later arrivals that do not contain first-order raylets (see Fig. 12b). However, the reflection or refraction case is less computationally demanding, because intermediate points are constrained to lie on the interface. Mode conversions could also be found using this approach; for instance, using a *P*-wave velocity structure for the incident path and an *S*-wave velocity structure for the reflected path will produce a *P*–*S* conversion.

The use of reciprocal traveltime fields to extract raylets and hence later arrivals has the added benefit of providing information on Fresnel volumes. In the simple case of Fig. 3(c), the contours that encapsulate the first-arrival can be viewed as the bounds of the first Fresnel volume for waves of different frequency. The later-arrivals also exhibit this feature, but since first-arrival traveltime fields are used, the Fresnel volumes are incomplete. Later-arrival traveltime fields are required to build the full Fresnel volumes for these rays. In previous work, Husen & Kissling (2001) use the contours of reciprocal traveltime fields, calculated using the eikonal solver of Podvin & Lecomte (1991), to locate so-called 'fat-rays', which are rays of finite-width defined by the first Fresnel volume. Husen & Kissling (2001) apply the new technique to local earthquake tomography to account for the finite frequency effects of wave propagation. This approach represents an interesting alternative to the more common methods for estimating Fresnel volumes such as paraxial ray theory (e.g. Červený & Soares 1992).

Another area in which forward and reciprocal rays are used is in applications of Kirchhoff theory, such as the migration of reflection data or the computation of synthetic seismograms. For example, Haddon & Buchen (1981) compute global body wave seismograms using a scheme based on the Kirchhoff integral representation of scalar waves. This requires rays to be traced from a source and receiver to an intervening surface over which an integration is performed based on traveltime isochrons. The traveltime surface is essentially a slice through the summed source and reciprocal traveltime fields, and stationary points on this surface can be viewed as raylet cross-sections. Cao & Kennett (1989) develop a similar scheme to Haddon & Buchen (1981) for reflection seismograms. In this case, traveltime isochrons are contoured on reflector surfaces by shooting rays from both the source and receiver to the reflector.

Although we have applied FORM in 2-D, the extension to 3-D is straightforward, as none of the principles involved or proofs are dependent on the dimensionality of the model. Raylets are delineated in exactly the same manner and remain stationary paths within the summed traveltime field. One simply needs a 3-D grid-based traveltime solver to compute the source time field and reciprocal time field throughout the model volume. Stationary curves and path segments can then be located in exactly the same way as before. The compute cost would essentially scale with the number of points used to describe the medium. This stands in stark contrast to WFC, which needs sophisticated surface evolution algorithms to properly track an evolving wave front in 3-D (e.g. Vinje *et al.* 1999) with computational demands increasing accordingly.

From a practical implementation point of view, a raylet-based scheme can in principle use any method to calculate the first-arrival traveltime field, be it an eikonal solver, shortest path method or some other approach. Minimal changes should be required to adapt any of the currently available techniques. Of course, further work is required to develop a practical scheme that can find all arrivals. Although seismology is one obvious area of application, raylet theory

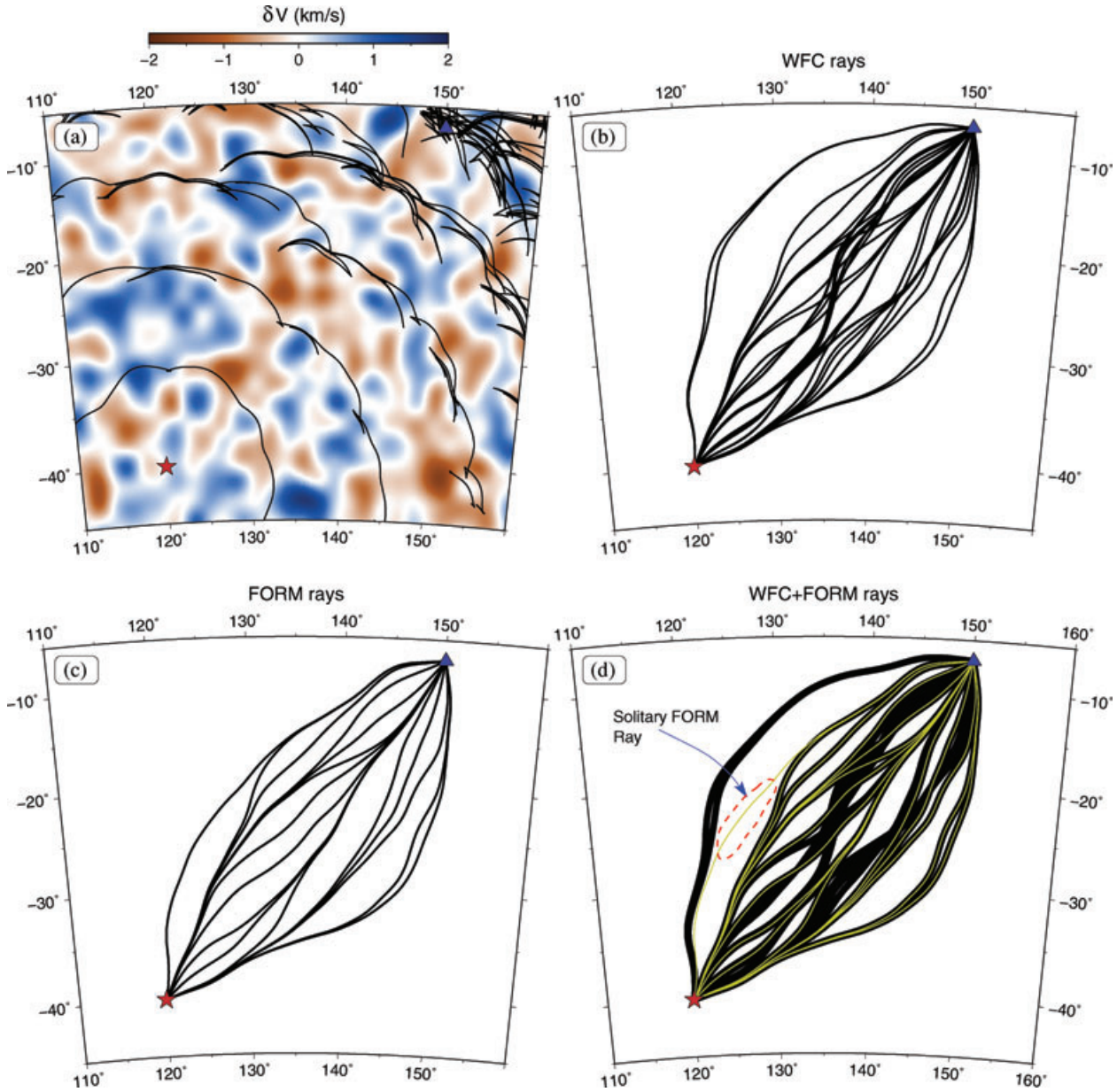

Figure 16. Application of WFC in the presence of a complex velocity model. (a) Snapshots of the complete multi-valued wave front (at 200 s intervals); (b) all WFC ray paths; (c) all FORM ray paths; (d) all FORM ray paths (yellow) superimposed on all WFC ray paths (black).

Table 1. Comparison of WFC and FORM multiarrival traveltimes.

		Traveltime difference ($\times 10^{-3}$% or parts in 10^5)						Sampling parameters	
Scheme	CPU time (s)	Arrival 1	Arrival 2	Arrival 3	Arrival 4	Arrival 5	Arrival 6	No. of FMM grid points	
FORM1	0.89	6.41	0.50	4.10	0.56	3.36	1.90	337,561	
FORM2	3.45	1.88	0.12	1.13	0.03	1.45	10.54	1,347,921	
FORM3	14.84	0.57	0.35	0.35	0.20	0.57	17.20	5,387,041	
								Time step (s)	No. points
WFC1	1.13	20.96	259.98	252.05	15.95	52.47	230.89	2.00	60
WFC2	3.68	7.46	21.05	37.65	5.82	5.28	36.30	1.00	150
WFC3	15.31	2.45	9.04	9.46	2.41	0.45	12.26	0.50	250
Reference time (s)		1060.852	1183.481	1192.245	1196.191	1205.793	1214.862	0.05	1000

Note: The "No. points" label at the bottom right-hand corner of the table refers to the number of points used to describe the wave front at the source point. Calculations are made on an Intel Core i7 workstation with 6 Gb RAM and a 64-bit Linux Operating system. gfortran is used to compile both codes, which are written in Fortran 90.

applies to any area of the physical sciences in which geometric ray theory is a valid approximation.

ACKNOWLEDGMENTS

This work was supported by Australian Research Council Discovery Project DP098675. B. L. N. Kennett is thanked for providing useful comments on a draft version of this paper.

REFERENCES

Afnimar & Koketsu, K., 2000. Finite difference traveltime calculation for head waves travelling along an irregular interface, *Geophys. J. Int.,* **143,** 729–734.

Benamou, J.D., 1996. Big ray tracing: multivalued travel time field computation using viscosity solutions of the Eikonal equation, *J. Comp. Phys.,* **128,** 463–474.

Benamou, J.D., 1999. Direct computation of multivalued phase space solutions for Hamilton–Jacobi equations, *Commun. Pure appl. Math.,* **52,** 1443–1475.

Benamou, J.D., 2003. An introduction to Eulerian Geometrical Optics (1992–2002), *SIAM J. Sci. Comput.,* **19,** 63–93.

Bevc, D., 1997. Imaging complex structures with semirecursive Kirchhoff migration, *Geophysics,* **62,** 577–588.

Cao, S. & Greenhalgh, S., 1994. Finite-difference solution of the eikonal equation using an efficient, first-arrival, wavefront tracking scheme, *Geophysics,* **59,** 632–643.

Cao, S. & Kennett, B.L.N., 1989. Reflection seismograms in a 3-D elastic model: an isochronal approach, *Geophys. J. Int.,* **99,** 63–80.

Capon, J., 1971. Comparison of Love- and Rayleigh-wave multipath propagation at LASA, *Bull. seism. Soc. Am.,* **61**(5), 1327–1344.

Červený, V., 2001. *Seismic Ray Theory,* Cambridge University Press, Cambridge.

Červený, V. & Soares, J.E.P., 1992. Fresnel volume ray racing, *Geophysics,* **57,** 902–915.

Chambers, C.J. & Kendall, J.M., 2008. A practical implementation of wave front construction for 3-d isotropic media, *Geophys. J. Int.,* **174,** 1030–1038.

Chang, Y.C., Hou, T.Y., Merriman, B. & Osher, S., 1996. A level set formulation of Eulerian interface capturing methods for incompressible fluid flows, *J. Comput. Phys.,* **124,** 449–464.

Cheng, L.-T., 2007. Efficient level set methods for constructing wavefronts in three spatial dimensions, *J. Comput. Phys.,* **226,** 2250–2270.

Cheng, N. & House, L., 1996. Minimum traveltime calculations in 3-D graph theory, *Geophysics,* **61,** 1895–1898.

Cockburn, B., Qian, J., Reitich, F. & Wang, J., 2005. An accurate spectral/discontinuous finite-element formulation of a phase-space-based level set approach to geometrical optics, *J. Comput. Phys.,* **208,** 175–195.

de Kool, M., Rawlinson, N. & Sambridge, M., 2006. A practical grid based method for tracking multiple refraction and reflection phases in 3D heterogeneous media, *Geophys. J. Int.,* **167,** 253–270.

Engquist, B. & Runborg, O., 2003. Computational high frequency wave propagation, *Acta Numerica,* **12,** 181–266.

Engquist, B., Runborg, O. & Tornberg, A.-K., 2002. High-frequency wave propagation by the segment projection method, *J. Comput. Phys.,* **178,** 373–390.

Ettrich, N. & Gajewski, D., 1996. Wave front construction in smooth media for prestack depth migration, *Pageoph,* **148,** 481–502.

Farra, V. & Madariaga, R., 1988. Non-linear reflection tomography, *Geophys. J.,* **95,** 135–147.

Fischer, R. & Lees, J.M., 1993. Shortest path ray tracing with sparse graphs, *Geophysics,* **58,** 987–996.

Fomel, S. & Sethian, J.A., 2002. Fast-phase space computation of multiple arrivals, *Proc. Natl. Acad. Sci. U.S.A.,* **99,** 7329–7334.

Haddon, R.A.W. & Buchen, P.W., 1981. Use of Kirchhoff's formula for body wave calculations in the Earth, *Geophys. J. R. astr. Soc.,* **67,** 587–598.

Hauser, J., Sambridge, M. & Rawlinson, N., 2008. Multiarrival wavefront tracking and its applications, *Geochem. Geophys. Geosyst.,* **9,** doi:10.1029/2008GC002069.

Hole, J.A. & Zelt, B.C., 1995. 3-D finite-difference reflection travel times, *Geophys. J. Int.,* **121,** 427–434.

Husen, S. & Kissling, E., 2001. Local earthquake tomography between rays and waves: fat ray tomography, *Phys. Earth planet. Inter.,* **123,** 129–149.

Julian, B.R. & Gubbins, D., 1977. Three-dimensional seismic ray tracing, *J. Geophys.,* **43,** 95–113.

Koketsu, K. & Sekine, S., 1998. Pseudo-bending method for three-dimensional seismic ray tracing in a spherical earth with discontinuities, *Geophys. J. Int.,* **132,** 339–346.

Lambaré, G., Lucio, P.S. & Hanyga, A., 1996. Two-dimensional multivalued traveltime and amplitude maps by uniform sampling of a ray field, *Geophys. J. Int.,* **125,** 584–598.

Leung, S., Osher, S.J. & Qian, J., 2004. A level set method for three-dimenstional paraxial geometrical optics with multiple point sources., *Commun. Math. Sci.,* **2,** 643–672.

Lucio, P.S., Lambaré, G. & Hanyga, A., 1996. 3D multivalued travel time and amplitude maps, *Pageoph,* **148,** 449–479.

Matsuoka, T. & Ezaka, T., 1992. Ray tracing using reciprocity, *Geophysics,* **57,** 326–333.

Moser, T.J., 1991. Shortest path calculation of seismic rays, *Geophysics,* **56,** 59–67.

Mulder, W., Osher, S. & Sethian, J.A., 1992. Computing interface motion in compressible gas dynamics, *J. Comput. Phys.,* **100,** 209–228.

Nakanishi, I. & Yamaguchi, K., 1986. A numerical experiment on nonlinear image reconstruction from first-arrival times for two-dimensional island arc structure, *J. Phys. Earth,* **34,** 195–201.

Osher, S. & Sethian, J., 1988. Fronts propagating with curvature dependent speed: algorithms based on hamilton-jacobi formuations, *J. Comput. Phys.,* **79,** 12–49.

Osher, S., Cheng, L.-T., Kang, M., Shim, H. & Tsai, Y.-H., 2002. Geometric optics in a phase-space-based level set and Eulerian framework, *J. Comput. Phys.,* **179,** 622–648.

Pereyra, V., Lee, W.H.K. & Keller, H.B., 1980. Solving two-point seismic-ray tracing problems in a heterogeneous medium, *Bull. seism. Soc. Am.,* **70,** 79–99.

Podvin, P. & Lecomte, I., 1991. Finite difference computation of traveltimes in very contrasted velocity models: a massively parallel approach and its associated tools, *Geophys. J. Int.,* **105,** 271–284.

Popovici, A.M. & Sethian, J.A., 2002. 3-D imaging using higher order fast marching traveltimes, *Geophysics,* **67,** 604–609.

Qin, F., Luo, Y., Olsen, K.B., Cai, W. & Schuster, G.T., 1992. Finite-difference solution of the eikonal equation along expanding wavefronts, *Geophysics,* **57,** 478–487.

Rawlinson, N. & Sambridge, M., 2004a. Wavefront evolution in strongly heterogeneous layered media using the fast marching method, *Geophys. J. Int.,* **156,** 631–647.

Rawlinson, N. & Sambridge, M., 2004b. Multiple reflection and transmission phases in complex layered media using a multistage fast marching method, *Geophysics,* **69,** 1338–1350.

Rawlinson, N., Houseman, G.A. & Collins, C.D.N., 2001. Inversion of seismic refraction and wide-angle reflection traveltimes for 3-D layered crustal structure, *Geophys. J. Int.,* **145,** 381–401.

Rawlinson, N., Hauser, J. & Sambridge, M., 2007. Seismic ray tracing and wavefront tracking in laterally heterogeneous media, *AG,* pp. 203–267.

Riahi, M.A. & Juhlin, C., 1994. 3-D interpretation of reflected arrival times by finite-difference techniques, *Geophysics,* **59,** 844–849.

Sambridge, M., 1999a. Geophysical inversion with a Neighbourhood algorithm —I. Searching parameter space, *Geophys. J. Int.,* **138,** 479–494.

Sambridge, M., 1999b. Geophysical inversion with a Neighbourhood algorithm -II. Appraising the ensemble, *Geophys. J. Int.,* **138,** 727–746.

Sambridge, M.S., 1990. Non-linear arrival time inversion: constraining velocity anomalies by seeking smooth models in 3-D, *Geophys. J. Int.,* **102,** 653–677.

Sethian, J.A., 1996. A fast marching level set method for monotonically advancing fronts, *Proc. Natl. Acad. Sci. U.S.A.,* **93,** 1591–1595.

Sethian, J.A. & Popovici, A.M., 1999. 3-D traveltime computation using the fast marching method, *Geophysics,* **64,** 516–523.

Steinhoff, J., Fan, M. & Wang, L., 2000. A new Eulerian method for the computation of propagating short acoustic and electromagnetic pulses, *J. Comput. Phys.,* **157,** 683–706.

Sun, Y., 1992. Computation of 2D multiple arrrival traveltime fields by an interpolative shooting method, *SEG Technical Program Expanded Abstracts,* pp. 1320–1323.

Symes, W.W. & Qian, J., 2003. A slowness matching eulerian method for multivalued solutions of eikonal equaions, *SIAM J. Sci. Comput.,* **19,** 501–526.

Um, J. & Thurber, C., 1987. A fast algorithm for two-point seismic ray tracing, *Bull. seism. Soc. Am.,* **77,** 972–986.

Velis, D.R. & Ulrych, T.J., 1996. Simulated annealing two-point ray tracing, *Geophys. Res. Lett.,* **23,** 201–204.

Vidale, J.E., 1988. Finite-difference calculations of traveltimes, *Bull. seism. Soc. Am.,* **78,** 2062–2076.

Vidale, J.E., 1990. Finite-difference calculations of traveltimes in three dimensions, *Geophysics,* **55,** 521–526.

Vinje, V., Iversen, E. & Gjøystdal, H., 1993. Traveltime and amplitude estimation using wavefront construction, *Geophysics,* **58,** 1157–1166.

Vinje, V., Iversen, E., Åstebøl, K. & Gjøystdal, H., 1996. Estimation of multivalued arrivals in 3D models using wavefront construction—Part I, *Geophys. Prospect.,* **44,** 819–842.

Vinje, V., Åstebøl, K., Iversen, E. & Gjøystdal, H., 1999. 3-D ray modelling by wavefront construction in open models, *Geophys. Prospect.,* **64,** 1912–1919.

Williamson, P.R., 1990. Tomographic inversion in reflection seismology, *Geophys. J. Int.,* **100,** 255–274.

Xu, S. & Lambaré, G., 2004. Fast migration/inversion with multivalued rayfields: Part 1—Method, validation test, and application in 2D to Marmousi, *Geophysics,* **69,** 1311–1319.

Xu, S., Lambaré, G. & Calandra, H., 2004. Fast migration/inversion with multivalued rayfields: Part 1—Applications to the 3D SEG/EAGE salt model, *Geophysics,* **69,** 1320–1328.

Zhao, A., Zhongjie, Z. & Teng, J., 2004. Minimum travel time tree algorithm for seismic ray tracing: improvement in efficiency, *J. geophys. Eng.,* **1,** 245–251.

Zhao, D., Hasegawa, A. & Horiuchi, S., 1992. Tomographic imaging of *P* and *S* wave velocity structure beneath Northeastern Japan, *J. geophys. Res.,* **97,** 19 909–19 928.